Molecular Therapy
Oncolytics
Original Article

miR-7 Reduces Breast Cancer Stem Cell Metastasis via Inhibiting RELA to Decrease ESAM Expression

Miao Li,[1,5] Meng Pan,[1,2,5] Jing Wang,[3,5] Chengzhong You,[4] Fengshu Zhao,[1] Danfeng Zheng,[1] Mei Guo,[1] Hui Xu,[1,3] Di Wu,[3] Ling Wang,[1] and Jun Dou[1]

[1]Department of Pathogenic Biology and Immunology, School of Medicine, Southeast University, Nanjing 210009, China; [2]Jiangsu Province Hospital, The First Affiliated Hospital of Nanjing Medical University, Nanjing 210029, China; [3]Department of Gynecology & Obstetrics, Zhongda Hospital, School of Medicine, Southeast University, Nanjing 210009, China; [4]Department of General Surgery, Zhongda Hospital, School of Medicine, Southeast University, Nanjing 210009, China

This study aimed to present evidence that miR-7 inhibited the metastasis of breast cancer stem cells (BCSCs) and elucidated the mechanisms that have remained unknown. The samples collected from miR-7 agomir-treated, BCSC-driven tumors were subjected to a protein array to analyze the protein expression profiles. A dual-luciferase reporter and chromatin immunoprecipitation-PCR were used to validate and evaluate the molecular expressions of interest in the collected breast cancer tissues and cell lines. miR-7 overexpression affecting metastasis of BCSCs was further evaluated in mice. The endothelial cell-selective adhesion molecule (ESAM) was highly expressed in breast cancer tissues and in BCSC-driven xenografts. Results of the dual-luciferase reporter and chromatin immunoprecipitation-PCR indicated that the miR-7 mimic reduced RELA expression by directly targeting the 3′ UTR of RELA to inhibit ESAM expression in MDA-MB-231 cells. Moreover, the expression levels of RELA, CD44, and ESAM were significantly decreased in lentivirus (Lenti)-miR-7-BCSC-driven xenografts compared with the control xenografts, accompanied with an increase in E-cadherin and a decrease in vimentin expression, as well as reduction in tumor growth and metastasis to lungs. Our data demonstrated that miR-7 overexpression reduced the metastasis of BCSCs via inhibiting ESAM, suggesting that ESAM could be a potential target for breast cancer therapy.

INTRODUCTION

Numerous recent studies have focused on new treatment strategies that combine surgery, radiotherapy, chemotherapy, and biotherapy to treat breast cancer patients. However, approximately 25% of breast cancer patients who are clinically node-negative at diagnosis eventually have cancer recurrence.[1,2] A possible reason is that there are breast cancer stem cells (BCSCs) in the tumors. BCSCs represent only a small fraction of tumor cells that can regenerate tumor through aberrant proliferation and self-renewal, resulting in metastasis and relapse of breast cancer. However, the biological features of BCSCs and the metastatic potential still remain to be elucidated.[3] Therefore, a successful breast cancer therapy may require a strategy against metastasis of BCSCs by using special therapies.[4–6]

Evidence from a recent study has shown that the endothelial cell-selective adhesion molecule (ESAM), a member of the immunoglobulin receptor family, mediates homophilic interactions between endothelial cells.[7] ESAM might be involved in modulating vascular endothelial growth factor-dependent action and regulating tumor metastasis through endothelial cell migration and tube formation in metastatic nodules.[8] In this regard, inhibition of ESAM might suppress cancer metastasis by inhibiting the angiogenic processes.[9]

Studies have suggested that a noncoding microRNA (miRNA), miR-7, is a cancer inhibitor and that enforced miR-7 expression significantly reduced the self-renewal ability of BCSCs.[10,11] In our previous study, we found that miR-7 was downregulated in BCSCs compared with the non-BCSCs analyzed by the miRNA microarray (confirmed by quantitative real-time PCR), and that miR-7 mediated downregulation of SET domain bifurcated 1, a new oncogene that was overexpressed in breast cancer, and inhibited tumor progression and metastasis in a BCSC-driven tumor xenograft mouse model.[11] However, the exact molecular mechanisms remain largely unknown.

In the present study, we focused on the effects of enforced miR-7 expression on inhibition of the metastasis of $CD44^+CD24^-ESA^+$ BCSCs and sought to clarify its molecular mechanisms in the BCSC-derived tumor xenografts in nonobese diabetic (NOD)/severe combined immunodeficient (SCID) mice.

The results of a protein array from the study indicated that high ESAM and yet low miR-7 expression levels were found in the BCSC-driven xenografts. Additionally, results of quantitative real-time PCR showed that ESAM expression was significantly higher in

Received 2 April 2020; accepted 1 June 2020;
https://doi.org/10.1016/j.omto.2020.06.002.

[5]These authors contributed equally to this work.

Correspondence: Jun Dou. Department of Pathogenic Biology and Immunology, School of Medicine, Southeast University, 87 Ding Jiaqiao Road, Nanjing 210009, China.
E-mail: njdoujun@seu.edu.cn

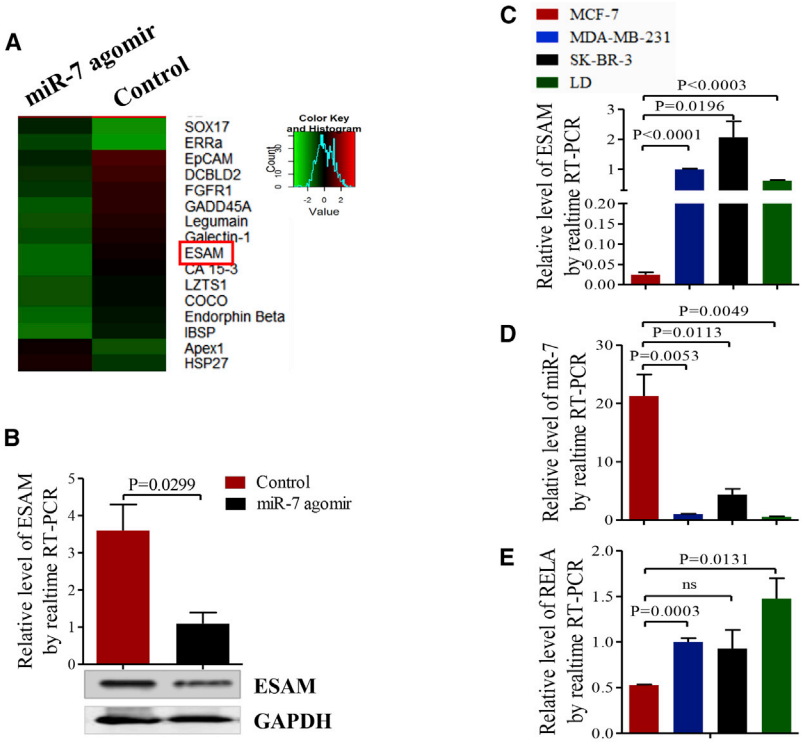

Figure 1. Results of Protein Array and Identification of Interested Molecular Expression

(A) Heatmap of protein array scanning analysis was generated for the protein expression in the $CD44^{+}CD24^{-}ESA^{+}$ BCSC-driven tumor tissues of mice treated with miR-7 agomir or PBS. (B) ESAM expression in the miR-7 agomir and control groups. (C–E) Validation expression levels of (C) ESAM, (D) miR-7, and (E) RELA in MCF-7, SK-BR-3, MDA-MB-231, and LD cells by quantitative real-time PCR.

breast cancer tissues than in adjacent noncancerous tissues. Overexpression of miR-7 specifically inhibited RELA expression and led to a reduction in ESAM expression, which attenuated the tumorigenesis and lung metastasis of BCSCs. The data suggested that the targeted inhibition of ESAM reduced the lung metastasis of BCSC-driven xenografts and enhanced the efficacy of treatment of breast cancer.

RESULTS

miR-7 Influences Stem-like Molecular Expression in BCSC-Driven Xenografts

In an attempt to know the protein expression difference in tumor tissues between the miR-7 agomir and the PBS-treated BCSC-driven xenografts in NOD/SCID mice, we analyzed protein expression profiling by protein array. Figure S1 gives results of protein array scanning. It indicates that 55 proteins were differentially expressed, including 21 with upregulated expression and 34 with downregulated expression in 493 target proteins compared with the control. Figure 1B shows that ESAM expression was significantly downregulated in miR-7 agomir-treated, BCSC-driven tumor tissues compared with PBS-treated, BCSC-driven tumor tissues ($p < 0.0299$), which was consistent with results of the protein array in Figure 1A. The different protein expression profiling is listed in Table S6.

To further identify ESAM expression, we detected its expression in MCF-7, SK-BR-3, MDA-MB-231, and LD cell lines. As shown in Figures 1C and 1D, ESAM expression in MCF-7 cells was significantly decreased compared to MDA-MB-231 ($p < 0.001$), SK-BR-3 ($p < 0.0179$), and LD ($p < 0.01$) cells, respectively, whereas the miR-7 expression in MCF-7 cells was significantly increased compared with MDA-MB-231 ($p < 0.0053$), SK-BR-3 ($p < 0.0113$), and LD ($p < 0.0053$) cells, respectively. Owing to the role of RELA in the stem-like molecule expression,[12,13] we simultaneously detected RELA expression. High RELA expression was found in MDA-MB-231, SK-BR-3, and LD cells (Figure 1E), which was consistent with ESAM expression pattern.

Expression Levels of ESAM, miR-7, and RELA in Breast Cancer Patients

After having validated the expression levels of ESAM and miR-7 in a mouse xenograft model and in human breast cancer cell lines, we further investigated these levels in breast cancer. To this end, we collected 12 postsurgery samples from breast cancer patients and used them in a quantitative real-time PCR assay. From the results in Figure 2A, we found that the expression of ESAM was significantly higher in breast cancer tissues than in adjacent normal tissues, whereas the miR-7 expression was markedly lower than in adjacent normal tissues, which was statistically significant ($p = 0.0087$ or $p = 0.0227$). Figure 2A also indicates that RELA expression was remarkably higher in breast cancer tissues than in adjacent normal tissues ($p = 0.0125$). Figure 2B indicates that the lower was the miR-7 expression, the higher was the ESAM expression, which was statistically significant ($p = 0.0104$, $r = -0.7015$), but the relative expression levels of ESAM and RELA changed simultaneously ($p = 0.0318$, $r = 0.6192$) (Figure 2C). Additionally, western blot analyses showed that the expression levels of RELA, phosphorylated (p-)RELA, and ESAM were remarkably higher in breast cancer tissues than in adjacent normal tissues (Figure 2D), which was statistically significant (Figure 2E).

miR-7 Inhibits ESAM Expression by Targeting RELA

Figure 2B suggests that expression levels of miR-7 and ESAM are negatively correlated. To confirm this relationship, we used the miR-7 mimic and the RELA small interfering RNA (siRELA) recombinants to transfect them into MDA-MB-231 and MCF-7 cells. We found that ESAM transcriptional (Figure 3A) and translational (Figure 3B) expression levels in MDA-MB-231 cells were significantly decreased in comparison with the different controls after miR-7 mimic transfection, which were statistically significant (Figures 3A and 3C). Figures 3D and 3E show that transcriptional and translational expression levels of ESAM were markedly reduced compared

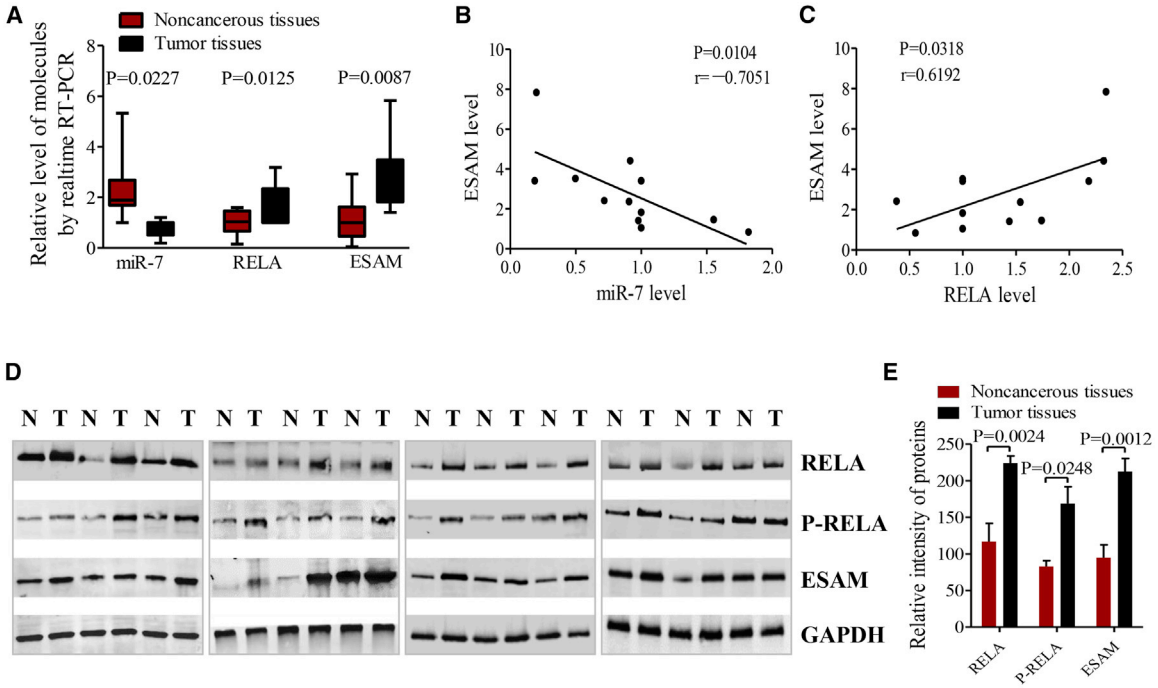

Figure 2. Analysis of Interested Molecular Expression in Breast Tumor Tissues of Patients

(A) Relative expression of miR-7, ESAM, and RELA were analyzed in breast tumor tissues and adjacent normal tissues of 12 patients by qRT-PCR. (B) Relative expression of miR-7 and ESAM. (C) Relative expression of RELA and ESAM. (D) Western blotting analysis of the expression of RELA, p-RELA, and ESAM. N, noncancerous tissues; T, tumor tissues. (E) Semiquantitative analysis of the protein expression of RELA, p-RELA, and ESAM; refer to the differences as indicated.

with the different controls after the siRELA recombinants were transfected into MDA-MB-231 cells, as shown in Figure 3D. In Figures 3G–3K, the transcriptional and translational expression levels of ESAM were also remarkably decreased compared to the different controls after miR-7 mimic and siRELA recombinants were transfected into MCF-7 cells, which were statistically significant (Figures 3I and 3L).

In addition, the RELA 3′ UTR contained two miR-7 binding sites (Figure 3M). Therefore, a dual-luciferase reporter assay was carried out in the MDA-MB-231 cells. We cloned the luciferase reporter assay vectors (psiCHECK2-RELA-3′ UTR-mutant [Mut] and psiCHECK2-RELA-3′ UTR) according to the sequences (Figure S2A), and then the luciferase reporter assay was performed as previously described.[11,14] Figure 3N indicates that the miR-7 mimic decreased the relative luciferase activity of the wild-type (WT) vector but not the relative luciferase activity of the mutation A or B vector or the A plus B vector.

Furthermore, we tested whether RELA had increased the occupancy in the promoter region of its target gene *ESAM* and performed a chromatin immunoprecipitation (ChIP) assay. Based on JASPAR database prediction, we found that there are four putative RELA binding sites in the *ESAM* promoter located at the −1232 to −1243, −1234 to −1244, −1345 to −1355, and −1545 to −1555 positions (Figure S2B). ChIP PCR results demonstrated that RELA was directly bound to the −1232 to −1243 region in the *ESAM* promoter 1 in MDA-MB-231 cells (Figure 3O).

Enforced miR-7 Expression Attenuates BCSC-Driven Tumor Growth and Inhibits Tumor Metastasis

After having demonstrating that the expression of ESAM was reduced in miR-7 mimic-transfected MDA-MB-231 and MCF-7 cells *in vitro*, we wanted to know whether miR-7 could have an effect on ESAM expression and attenuate BCSC-driven tumor growth and metastasis *in vivo*. To this end, we established a BCSC-driven xenograft model by local injection of lentivirus (Lenti)-miR-7-BCSCs (2×10^5), which were isolated from LD cells, into the NOD/SCID mouse's right inguinal mammary fat pads. As shown in Figure 4, the LD cell line was established in the present study from a postoperative human breast cancer tissue (diameter of 2.8 cm, infiltrating ductal carcinoma, TNM [tumor, node, metastasis] stage IIa [T2, N0, M0]), which was cultured in DMEM with 10% fetal bovine serum (FBS), day 16 (5×10) and day 21 (10×10), observed with microscopy (Figure 4A). To determine counts in BCSCs in LD cells, we used a flow cytometer (FCM) to analyze the ALDH1 activity (biological marker)[15] and $ESA^+CD44^+CD24^-$ cell phenotypes (surface markers). Figure 4B shows that the ALDH-positive cells accounted for 10.63% of the total of LD cells, and $ESA^+CD44^+CD24^-$ cell phenotypes accounted for 21.50% of the total of LD cells (Figure 4C). The result of sorting $ESA^+CD44^+/CD24^-$ cells (purity for 90.60%) is shown in Figure 4D. From

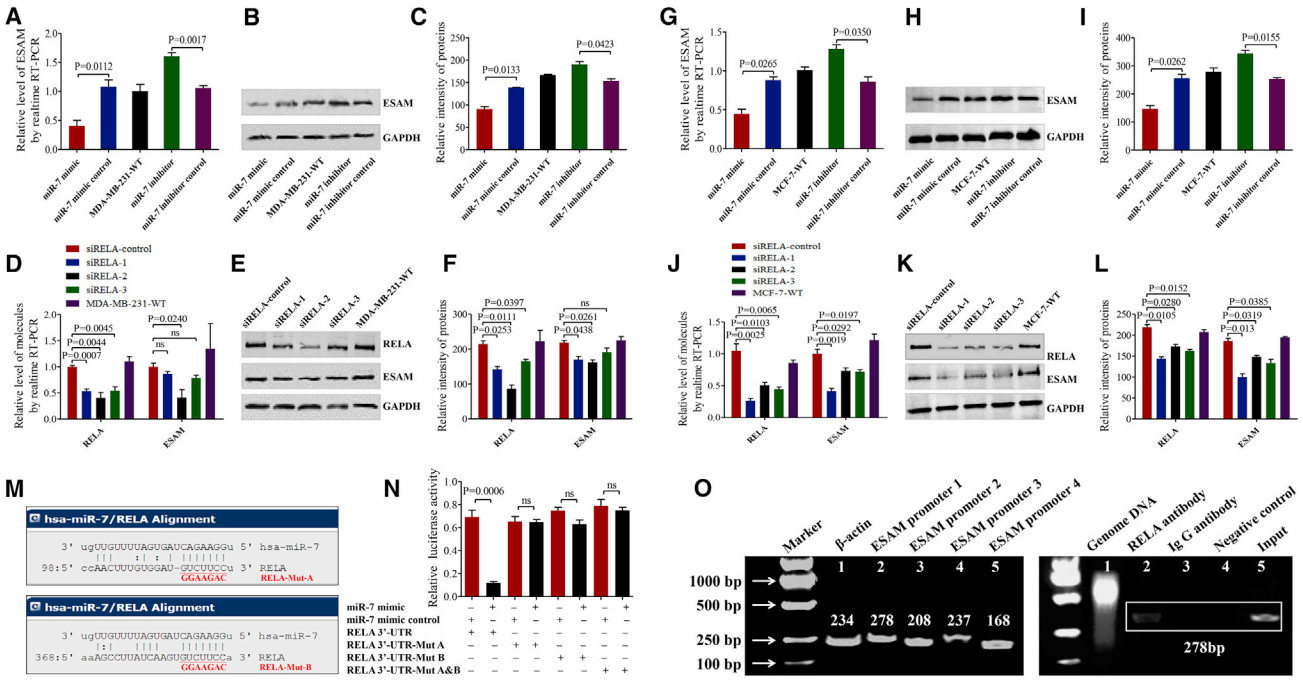

Figure 3. Effects of miR-7 Mimic and siRELA Recombinants on the Expressions of ESAM and RELA in MDA-MB-231 and MCF-7 Cells

(A and B) ESAM expression analyzed by (A) quantitative real-time PCR and (B) western blot in MDA-MB-231 cells transfected with a miR-7 mimic. (C) Quantification of ESAM translational expression in MDA-MB-231 cells. (D and E) ESAM and RELA expression analyzed by (D) quantitative real-time PCR and (E) western blot in MDA-MB-231cells transfected with various siRELA recombinants. (F) Quantification of ESAM and RELA translational expression. (G, H, J, and K) Relative expression of (G and H) ESAM and (J and K) RELA analyzed by (G and J) quantitative real-time PCR and (H and K) western blot in MCF-7 cells transfected with a miR-7 mimic and various siRELA recombinants, respectively. (I) Quantification of translational expression of ESAM in MCF-7 cells. (L) Quantification of translational expression of ESAM and RELA in MCF-7 cells. (M) Two miR-7 binding sites in the RELA 3′ UTR region. (N) Luciferase activity of the wild-type or mutant RELA 3′ UTR reporter genes in MDA-MB-231 cells transfected with miR-7 mimics or miR-7 mimics control or the different psiCHECK2-RELA-3′UTR-Mut vectors. (O) ChIP-PCR results.

these results, we concluded that LD cells have a high BCSC population for the sequent experiment *in vivo*.

Figure 5A shows images of LD cells and BCSC-driven tumor xenografts in mice. Figure 5B shows photographs of the sizes of tumors removed from the BCSC-driven xenograft in mice 31 days after the local injection. Owing to the $CD44^{+}CD24^{-}ESA^{+}$ BCSC origin of LD cells (Figure 4), BCSCs have a strong tumorigenicity. Accordingly, the injection of LD-BCSCs (2×10^{5}) without infection of Lenti-miR-7 quickly generated tumors on day 10, and tumor growth was the fastest 31 days after injection, whereas LD cells (2×10^{5}) generated tumors on day 16 after injection. In the Lenti-miR-7-LD-driven tumor group, only two of the four mice generated the smallest tumor on day 31 (Figure 5B), and tumor growth was the slowest among the all groups (Figure 5D). As shown in Figure 5E, the differences were statistically significant between the LD-BCSCs and the LD cells, and between the Lenti-miR-7 BCSCs and the other control groups.

We found that the $CD44^{+}$ cell percentages and the expression levels of CD44, RELA, p-RELA, and ESAM in tumor tissues were significantly decreased (Figures 5F and 5I); however, miR-7 expression was markedly increased in the Lenti-miR-7-BCSC group compared to the other three groups. In addition, the mouse weight was not changed remarkably in the Lenti-miR-7-BCSC group, and weight in this group was similar to that of control mice until day 31. This suggested that the Lenti-miR-7-BCSC did not cause severe side effects. However, in response to the combined adriamycin (Ad) plus cyclophosphamide (Cy) treatment, breast cancer-bearing mice showed a serious weight loss, suggesting severe side effects in mice treated with drugs (Figure 5C).

To identify the effect of enforced miR-7 expression on reducing BCSC-driven xenograft metastasis, we dissected lungs from the breast-cancer bearing mice on day 31 and tested for the presence of tumor micrometastasis as analyzed by H&E staining. We found more metastasized tumor nodules in the lungs of mice injected with BCSCs or BCSCs infected with lentiviral vector (Lentivector) than in the lungs of mice injected with Lenti-miR-7-infected BCSCs (Figure 6A). Differences in tumor nodules between the Lenti-miR-7-BCSC and Lentivector-BCSC groups, and between the Lenti-miR-7-BCSC group and the other control groups were found and are shown in Figure 6B.

To understand the mechanisms of miR-7 reducing the tumor xenograft metastasis, we detected the expression of epithelial-mesenchymal transition (EMT) characteristic molecules, which are closely

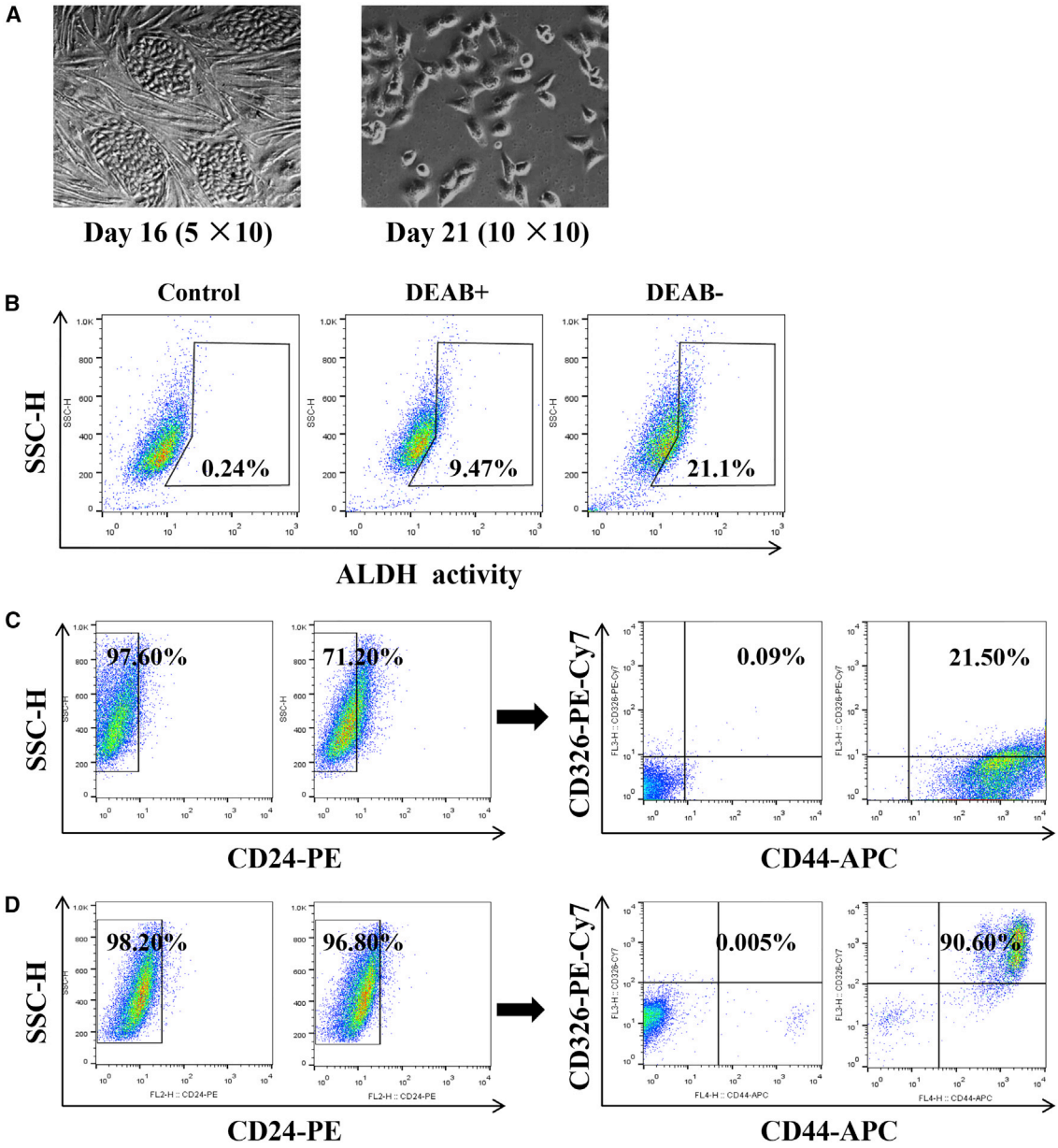

Figure 4. FCM Analyzes the BCSC Counts in LD Cells

The cells were set up from a breast cancer postsurgery sample. (A) Cells were cultured on day 16 (5 × 10) and day 21 (10 × 10), observed under microscopy. (B) ALDH activity cells were analyzed by FCM. (C) $ESA^+CD44^+CD24^-$ cell phenotypes in LD cells were analyzed by FCM. (D) Sorting of $ESA^+CD44^+CD24^-$ cells analyzed by FCM.

related to typical phenotype change of the tumor cell's EMT in a mouse model. Figure 6C shows expression levels of E-cadherin and vimentin in the tumor tissues analyzed by immunohistochemical staining. The tumor cells in mice injected with Lenti-miR-7-BCSCs significantly increased the staining of E-cadherin and markedly decreased the staining of vimentin compared to the tumor cells in mice injected with Lentivector-BCSCs, Lentivector-BCSCs-drugs, Lenti-miR-7-WT, LD-WT, and LD-BCSCs, respectively, which was statistically significant, as shown in Figures 6D and 6E.

Effects of Knockdown of ESAM on the Proliferation, Clone Formation, Metastasis, and BCSC-Driven Tumor Growth

Although we have demonstrated that enforced miR-7 expression reduced ESAM expression and attenuated BCSC-driven tumor growth, we wondered whether knockdown of ESAM affected MDA-MB-231 cell proliferation, colony, and metastasis *in vitro*, and inhibited BCSC-driven tumor growth in *in vivo* NOD/SCID mice by injection of siESAM-1. Figure 7A shows that the expression levels of ESAM mRNA and protein were significantly decreased in MDA-MB-231 cells

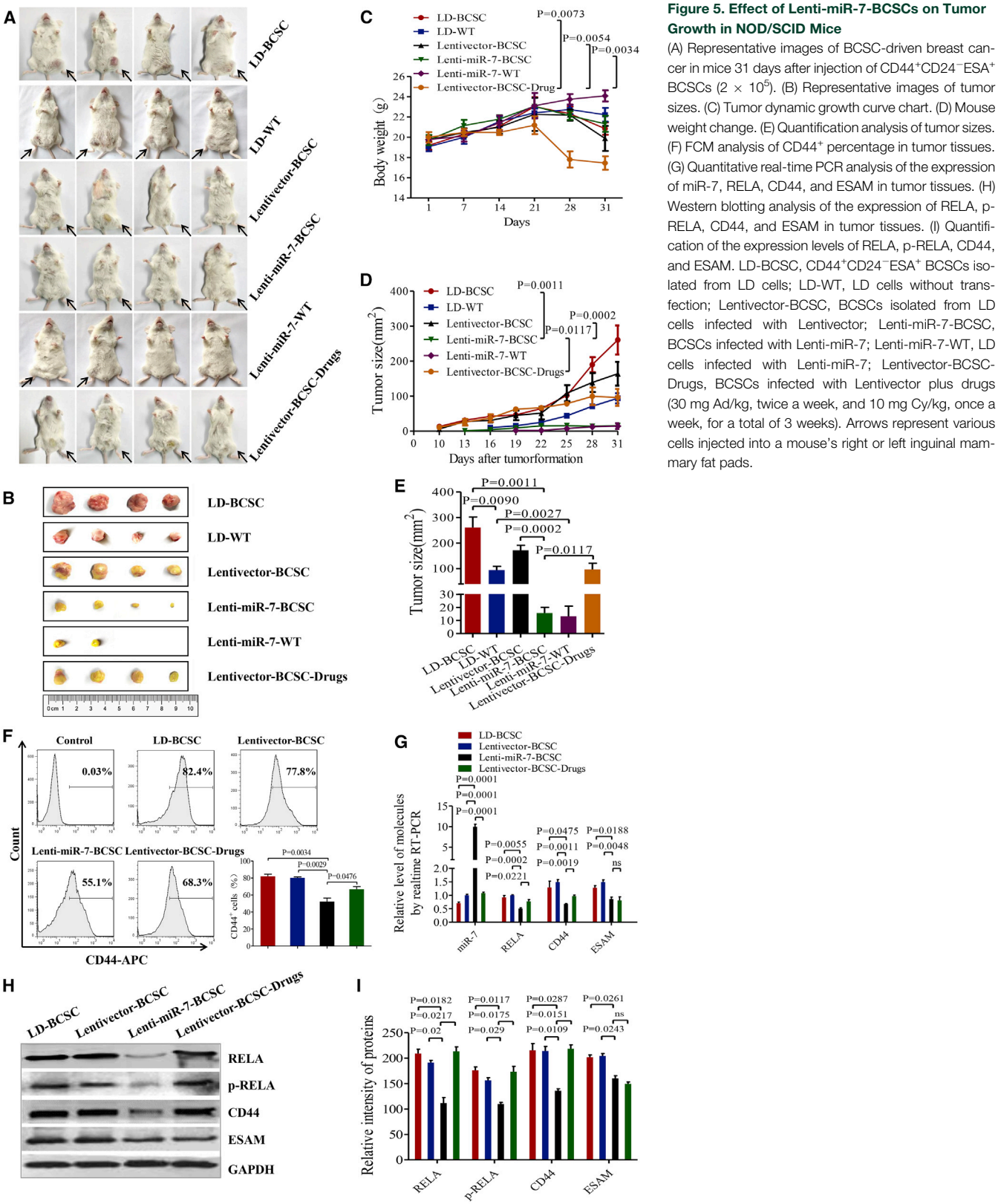

Figure 5. Effect of Lenti-miR-7-BCSCs on Tumor Growth in NOD/SCID Mice

(A) Representative images of BCSC-driven breast cancer in mice 31 days after injection of $CD44^+CD24^-ESA^+$ BCSCs (2×10^5). (B) Representative images of tumor sizes. (C) Tumor dynamic growth curve chart. (D) Mouse weight change. (E) Quantification analysis of tumor sizes. (F) FCM analysis of $CD44^+$ percentage in tumor tissues. (G) Quantitative real-time PCR analysis of the expression of miR-7, RELA, CD44, and ESAM in tumor tissues. (H) Western blotting analysis of the expression of RELA, p-RELA, CD44, and ESAM in tumor tissues. (I) Quantification of the expression levels of RELA, p-RELA, CD44, and ESAM. LD-BCSC, $CD44^+CD24^-ESA^+$ BCSCs isolated from LD cells; LD-WT, LD cells without transfection; Lentivector-BCSC, BCSCs isolated from LD cells infected with Lentivector; Lenti-miR-7-BCSC, BCSCs infected with Lenti-miR-7; Lenti-miR-7-WT, LD cells infected with Lenti-miR-7; Lentivector-BCSC-Drugs, BCSCs infected with Lentivector plus drugs (30 mg Ad/kg, twice a week, and 10 mg Cy/kg, once a week, for a total of 3 weeks). Arrows represent various cells injected into a mouse's right or left inguinal mammary fat pads.

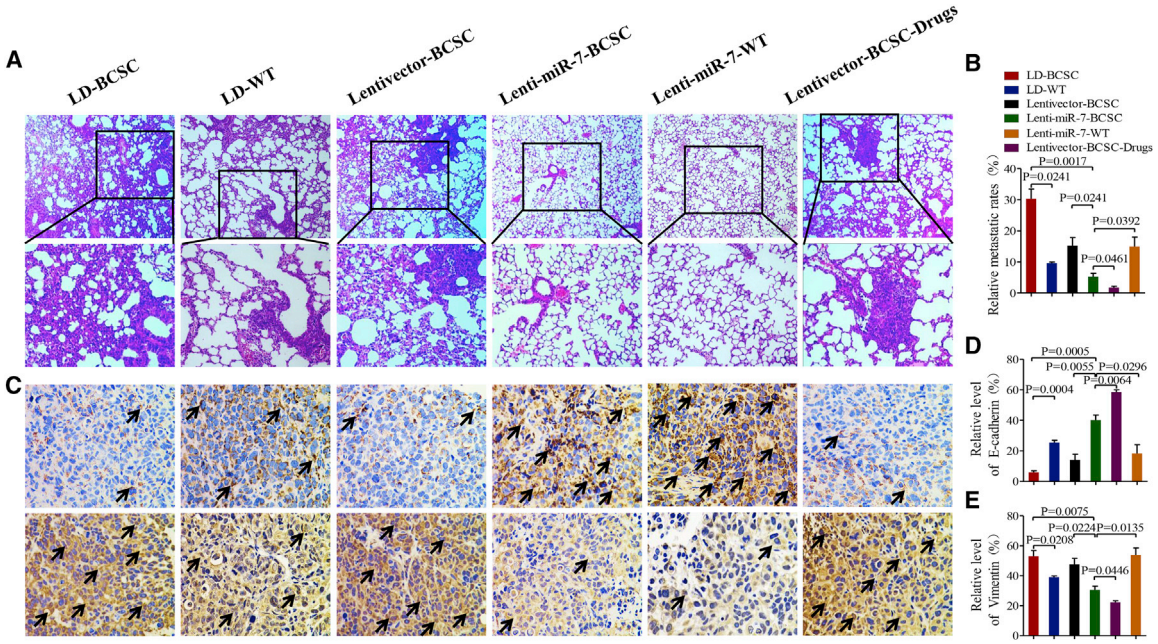

Figure 6. miR-7 Reduces Tumor Lung Metastasis

(A) Representative images of lung pathological sections stained with H&E are shown in the top panels (original magnification, ×100) and bottom panels (original magnification, ×200); the lung tissues were taken out of the BCSC-driven breast cancer in mice 31 days after injection of 2×10^5 BCSCs. (B) Semi-quantification of the tumor micrometastasis focus. (C) E-cadherin expression (top panels) and vimentin expression (bottom panels), analyzed by immunochemistry (original magnification, ×400). (D and E) Semi-quantification of the expression levels of (D) E-cadherin and (E) vimentin.

transfected with siESAM-1, siESAM-2, and siESAM-3 respectively, compared with the control cells, particularly in the siESAM-1-transfected cells. Figure 7B shows a lower proliferation rate in siESAM-1-transfected cells than in the other control cells, particularly in the 96-h culture. The difference was statistically significant between the siESAM-1 cells and the other control cells ($p < 0.001$). We also found that clone formation and metastasis were markedly reduced in siESAM-1-transfected cells compared to the other control cells, which was statistically significant (Figures 7C and 7D). Therefore, the synthetic siESAM-1 was used for subsequent *in vivo* study.

Figure 8A shows that the dynamic plot of mouse weight change, in which the siESAM-1-injected mice mostly maintained mouse weight similar to that of control mice, suggested that no severe side effects were caused. Figure 8B gives the tumor dynamic growth plot in mice. Figure 8C shows photographs of the BCSC-driven xenografts in mice on day 27 after implantation of $ESA^+CD44^+CD24^-$ BCSCs (2×10^5). Figure 8D includes photographs of tumor sizes. Tumor growth was significantly inhibited in mice injected with siESAM-1 compared with mice injected with LD-BCSCs or Lentivector-BCSCs, but the inhibitive effectiveness was still lower in mice than in mice injected with Lenti-miR-7-BCSCs, as shown in Figure 8E.

DISCUSSION

Emerging data demonstrate that BCSCs are typically seed cells of breast cancer and are involved in its metastasis and recurrence. However, the current treatment protocol for breast cancer may lack any approved molecular target therapy for the disease metastasis.[14] In the present study, we first investigated whether miR-7 could impact the metastasis-related molecular expression in miR-7 agomir-treated, $CD44^+CD24^-ESA^+$ BCSC-driven tumor xenograft tissues. The human L493 array provided by RayBiotech was used to assess protein expression profiles. Data of the protein array showed a novel molecule, ESAM, that was highly expressed in the BCSC-driven tumor tissues in mice treated with PBS, but it was lowly expressed in the BCSC-driven tumor tissues of mice treated with the miR-7 agomir. To verify the protein expression profiles, we used a variety of cell lines to analyze ESAM expression. Compared with the MCF-7 cell line, the MDA-MB-231, SK-BR-3, and LD cell lines exhibited high expression of ESAM and low expression of miR-7. It is known that MCF-7 cells are duct cell carcinoma with estrogen receptor (ER^+), progesterone receptor (PR^+), and epidermal growth factor receptor 2 ($HER2^-$),[16] while the MDA-MB-231 cells are $ER^-/PR^-/HER2^-$ (triple-negative breast cancer cells), the SK-BR-3 cells are $ER^-/PR^-/HER2^+$,[17,18] and the LD cells are $ER^+/PR^+/HER2^+$. Owing to the high expression of ESAM, a molecule tightly related to tumor cell metastasis, the cells with high ESAM expression may pose a higher capability of invasion and metastasis than do the MCF-7 cells, which are relative low malignancy.

To further verify the above results, we collected 12 breast samples from breast cancer patients to detect the expression of ESAM and

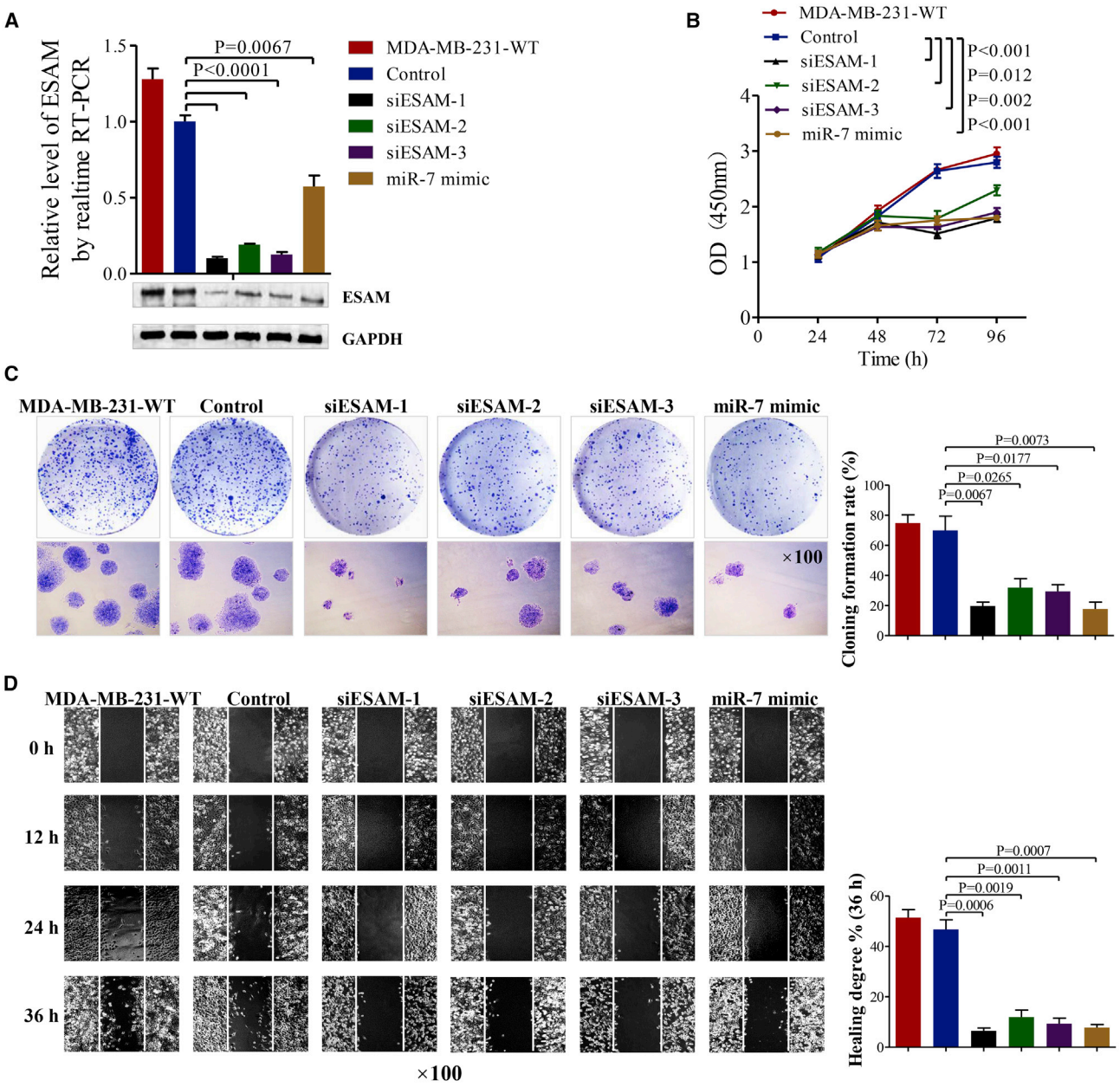

Figure 7. Inhibition of Proliferation, Metastasis, and Clonal Formation

(A) ESAM mRNA and protein expression in cells transfected with siESAMs. (B) Different cell dynamic proliferation curve chart. (C) Representative images of the different clones and statistical analysis of the clone formation rate. (D) Representative images of the different cell metastasis and statistical analysis of cell metastasis rate; refer to the differences as indicated.

miR-7 by quantitative real-time PCR. The results confirmed that, compared to the adjacent noncancerous tissues, the expression of ESAM was significantly increased in cancer tissues but miR-7 expression was markedly decreased. We also found that there is an inverse correlation between the expression levels of miR-7 and ESAM; alternatively, we found that RELA expression was positively correlated with ESAM expression in breast cancer tissues. Therefore, we further investigated the effects of miR-7 mimic and the siRELA recombinants on molecule expression in MDA-MB-231 and MCF-7 cells. Significantly, the transfection of miR-7 mimic or siRELA recombinants decreased the expression of ESAM. From these findings, we hypothesized that the decrease of ESAM expression may be due to direct regulation by miR-7 or RELA. To verify the hypothesis, we carried out dual-luciferase reporter and ChIP assays. As we had predicted,

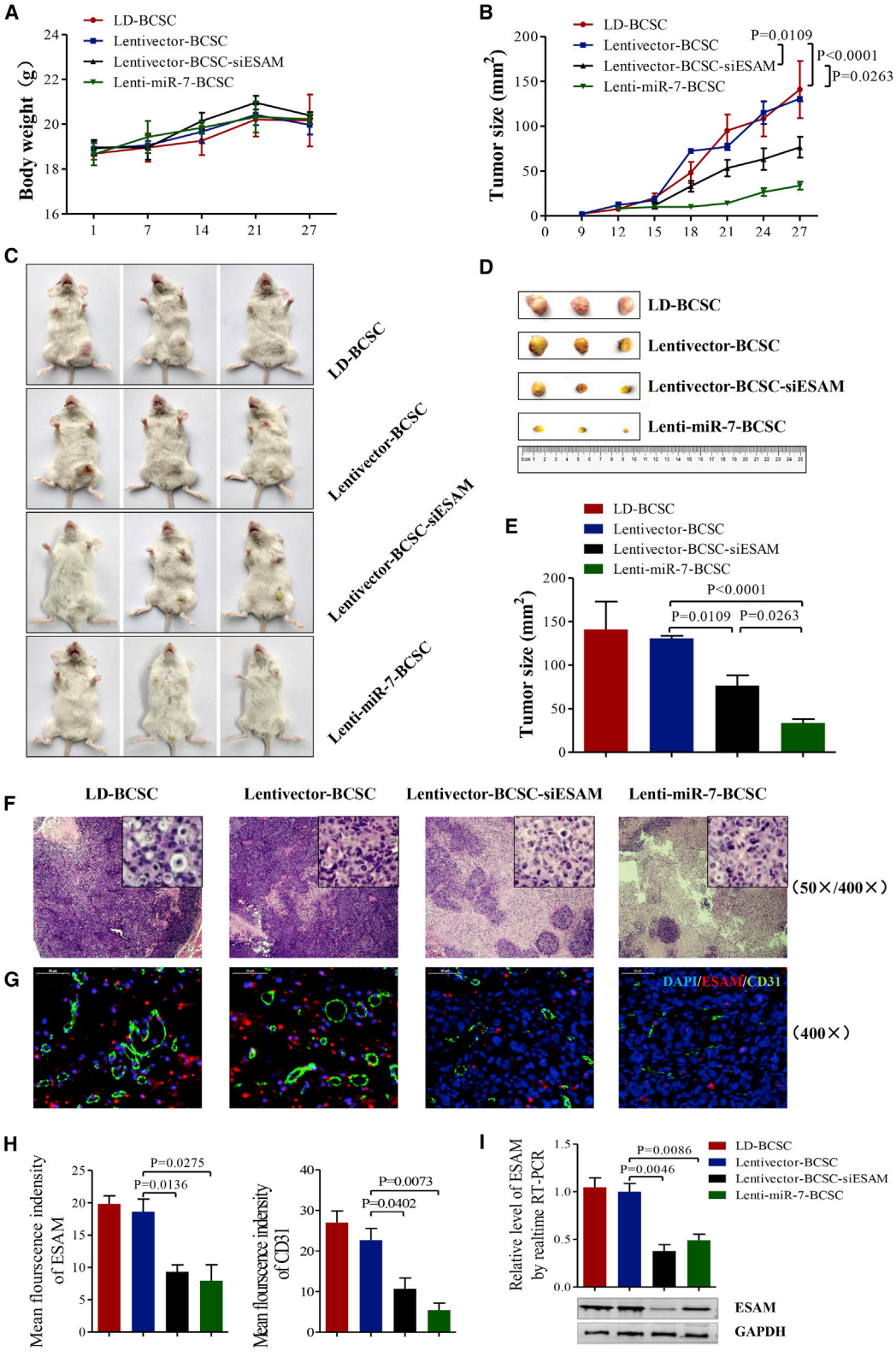

(legend on next page)

the dual-luciferase reporter assay indicated that miR-7 directly bound to the RELA 3′ UTR region. ChIP assays confirmed our hypothesis that RELA could directly bind to the region in the *ESAM* promoter that may enhance ESAM expression in MDA-MB-231 cells. It is thus evident that the miR-7 mimic indirectly inhibited ESAM expression by directly decreasing RELA expression.

More importantly, we observed that, in our *in vivo* animal experiment, the enforced miR-7 expression in BCSCs isolated from LD cells, which were established from the postoperative human breast cancer sample, not only reduced BCSC-driven tumor growth but also blocked tumor lung metastasis. This effect was better than that of the combination of Ad plus Cy treatment of breast cancer (one of the conventional therapies during the past few decades),[19] as was reflected in the slowed tumor growth, smaller tumor sizes, and almost no serious side effect, as well as no obvious tumor lung metastasis in the tumor-bearing mice. The FCM analyses indicated a decrease in cell percentage of the $CD44^+$ molecule, a surface marker for BCSCs, in the Lenti-miR-7-BCSC group. These results suggested that miR-7 overexpression reduced the BCSC subset and inhibited tumor growth and metastasis. In addition, the decreasing vimentin expression and yet increasing E-cadherin expression analyzed by immunohistochemical staining may be attributed to the reduced expression of ESAM, which was regulated by miR-7 that directly inhibited RELA expression in the BCSC-driven tumor tissues.[8,20]

It is known that ESAM is tightly associated with modulating tumor vascularization to promote tumor metastasis[8,9]; therefore, we investigated the effects of a direct knockdown of ESAM on MDA-MB-231 cell proliferation, clone formation, and metastasis *in vitro*, as well as on BCSC-driven xenograft growth in *in vivo* NOD/SCID mice by injection of a siESAM-1. Knockdown of ESAM expression in the MDA-MB-231 cells by injection of siESAM-1 not only inhibited cellular proliferation, clone formation, and metastasis *in vitro*, but it also inhibited the Lentivector-BCSC-driven xenograft growth in mice (Figures 8C and 8D), even though its inhibitive effect was slightly lower than that of the Lenti-miR-7-BCSC group. From the results of immunofluorescence analyses, we postulated that the local injection of siESAM-1 into tumor-bearing mice not only inhibited ESAM expression but also reduced the expression of CD31, a blood vessel marker, in the tumor tissue; this may have reduced tumor lung metastasis.

Conclusion

To our knowledge, the present study may be the first to delineate a novel molecular mechanism whereby ESAM was highly expressed in the $CD44^+CD24^-ESA^+$ BCSC-driven tumor xenografts and in breast cancer patients. Our *in vitro* and *in vivo* studies provide definitive evidence that the enforced miR-7 expression in BCSCs significantly inhibited tumor xenograft lung metastasis by miR-7 direct targeting of RELA to further inhibit ESAM expression. Our findings demonstrated that ESAM may serve as a specific target reducing BCSC distant metastasis via miR-7 overexpression.

MATERIALS AND METHODS

Cell Lines

Human breast cancer MCF-7, SK-BR-3, and MDA-MB-231 cell lines were obtained from the Cellular Institute in Shanghai, China. Cells were cultured in Dulbecco's modified Eagle's medium (DMEM) with 10% FBS. The LD cell line was established by our laboratory from a human breast cancer postsurgery sample that was cultured in DMEM with 10% FBS and characterized as shown in Figure 4. All media consist of 2 mM L-glutamine, 100 U/mL penicillin, 100 μg/mL streptomycin, and 10% FBS.

Infection with a Lentivirus-Encoding miR-7 Vector in LD Cells

To obtain the enforced miR-7 expression in $ESA^+CD44^+CD24^-$ BCSCs, a lentivirus-encoding miR-7 vector was infected into LD cells as previously described.[11,21] The clones with the stable miR-7 expression were selected by GFP expression.

Isolation and Identification of BCSCs

BCSC ALDH1 activity was identified with the ALDH1 enzyme assay kit (Invitrogen, Carlsbad, CA, USA), which was applied on an FCM. CD44/CD24 and CD44/CD24/ESA (also called EpCAM [epithelial cell adhesion molecule] or CD326) antibodies conjugated to magnetic microbeads (Miltenyi Biotec, Bergisch Gladbach, Germany) were used to obtain BCSCs from LD cell clones with stable miR-7 expression by a magnetic-activated cell sorting (MACS) system. LD cell clones was cultured in DMEM with 10% FBS; the isolated BCSCs from LD cell clones were directly injected into mice. The sorting method was performed by following the manufacturer's instructions and our previous study.[22–24] We named $CD44^+CD24^-ESA^+$ cells BCSCs.

Protein Array

Three independent controls and miR-7-treated tumor samples were used for the protein arrays, according to the standard operating procedures of the Raybio (USA) human L493 array (catalog no. AAH-BLG-2-2). Total protein was extracted from 250 mg of tissues with ice-cold cell & tissue protein extraction reagent (KangChen Bio-tech, China, catalog no. KC-415), which contained the inhibitors for protein degradation (5 μL of protease inhibitor cocktail, 5 μL of PMSF, and 5 μL of phosphotase cocktail were added into 1 mL of protein extraction reagent). The protein concentration was determined by a BCA protein assay kit (KangChen Bio-tech, catalog no.

Figure 8. siESAM-1 Inhibits the BCSC-Driven Tumor Growth in Mice

(A) Mouse weight dynamic plot. (B) The tumor dynamic growth plot in NOD/SCID mice. (C) The images of the BCSC-driven tumor mice injected with 2×10^5 ESA^+-$CD44^+CD24^-$ BCSCs. (D) Photographs of tumor sizes dissected from the differently treated mice on day 27. (E) Statistical analysis of tumor sizes. (F) HE staining of tumor tissues.(G) immunofluorescence detection of tumor tissues. (H) immunofluorescence analyses of ESAM and CD31. (I) ESAM expression analyzed by quantitative real-time PCR and western blot in tumors.

KC-430). Protein array membranes were blocked in blocking buffer for 30 min and then incubated with samples at room temperature for 1–2 h, then decanted, and membranes were washed with washing buffer. After that, membranes were incubated with diluted biotin-conjugated antibodies at room temperature for 1–2 h. The membranes were washed with washing buffer and reacted with streptavidin-conjugated fluor at room temperature. Membranes were then washed thoroughly and scanned by an Axon scanner. The intensities of signals were quantified by densitometry. Raw intensities were revised by background and normalized by median. A 2-fold change in protein expression was calculated.[25–27]

Animal Experiment

Female NOD/SCID mice at 6 weeks of age and weighing 18 ± 1 g were ordered from Beijing Weitong Lihua Experimental Animal Technology (China). All mice were raised in a specific pathogen-free (SPF) animal facility at the Experimental Animal Center, School of Medicine, Southeast University (Nanjing, Jiangsu, China). The animal experiments followed the guidelines of the Animal Research Ethics Board of Southeast University (China).

For the lentivirus miR-7 treatment experiment, each NOD/SCID mouse received inoculation of 2×10^5 LD-BCSCs, LD cells, Lentivector-LD-BCSCs, Lenti-miR-7-LD-BCSCs, Lenti-miR-7-LD cells, or Lentivector-LD-BCSCs plus drugs at the mouse's right or left inguinal mammary fat pads. Twenty-four mice were divided into six groups of equal size (four per group). Ten days after the injection, all mice grew tumors that reached 3–5 mm in size. At this time, the Lentivector-LD-BCSCs plus drugs group of mice alone received the following drugs: 30 mg/kg Ad (purchased from Dalian Meilun Biotech, China, twice a week for a total of 3 weeks) and 10 mg/kg Cy (purchased from Dalian Meilun Biotech, China), once a week for a total of 3 weeks in 0.1 mL of PBS; both were locally injected into the BCSC-formed tumor sites.

For the siESAM-1 treatment experiment (three per group), each NOD/SCID mouse received inoculation of 2×10^5 LD-BCSCs, Lentivector-LD-BCSCs, Lenti-miR-7- LD-BCSCs, or Lentivector-LD-BCSCs plus injection of siESAM-1, which was synthesized by Bioribo and performed as described previously, and 2 nmol of siESAM-1 in 0.1 mL of saline buffer was locally injected into the tumor site once every 3 days for a total of five times. The target sequences sited for siESAM are as follows: siESAM-1, 5′-GACAAACAAGG CAAATCTA-3′; siESAM-2, 5′-TGATGTGGTTCTTCAAACA-3′; siESAM-3, 5′-ACTGCCCAATGTAATGTGA-3′. Tumor take was assessed for up to 31 days. *In vivo* tumor growth in each mouse was monitored every 3 days by taking two-dimensional measurements of a tumor. The tumor tissues were subjected to western blotting, quantitative real-time PCR, hematoxylin and eosin (H&E), and immunohistochemistry assays.[28,29] The experiments were repeated twice.

Quantitative Real-Time PCR

To test the expression levels of miR-7, RELA, and ESAM, quantitative real-time PCR analyses were performed on an ABI StepOnePlus real-time PCR system (Applied Biosystems). Total cellular RNA was isolated from each sample by using a QIAGEN RNeasy kit (QIAGEN, Valencia, CA, USA). One microgram of total RNA per sample was subjected to cDNA synthesis using SuperScript III reverse transcriptase (Invitrogen). The mRNA levels of the genes of interest were expressed as the ratio of each gene of interest to U6 mRNA per sample. cDNAs were amplified by PCR with primers as listed in Table S1.[30]

Western Blot

Western blot was performed as described previously.[31,32] The rabbit anti-mouse/human nuclear factor κB (NF-κB) p65 (RELA) antibody (8242S) (Cell Signaling Technology, USA), the rabbit anti-mouse/human p-NF-κB p65 (RELA) antibody (AF2006) (Affinity Biosciences, USA), and the rabbit anti-mouse/human ESAM antibody (12445-1-AP) (Proteintech, USA) were used in the assay. Immunoreactive bands were detected by an Odyssey imaging system scanning instrument (LI-COR Biosciences, USA).

Breast Cancer Samples

Breast cancer postsurgery tissue samples were received from the Department of General Surgery of Zhongda Hospital at Southeast University (Nanjing, Jiangsu, China). Our study was approved by an Ethics Committee at Southeast University School of Medicine, together with confirmation that informed consent for the use of the postsurgery samples was obtained from the donors. The clinical data of 12 breast cancer patients and specimens are shown in Table S2.

Short Hairpin RNA Targeting the ESAM Encoding Gene

Short hairpin RNA sequences of a human RELA were designed based on the RELA DNA sequence (GenBank: NM_001128128.2) using siDESIGN software (Dharmacon, https://horizondiscovery.com/) and BLOCK-iT RNAi designer (Invitrogen, Grand Island, NY, USA) as well as BLAST (https://blast.ncbi.nlm.nih.gov/Blast.cgi).[33,34] The target sequence for RELA shRNA and one scramble sequence as a negative control are listed in Table S3. MDA-MB-231 cells were transiently transfected using Lipofectamine 2000 reagent (Invitrogen) according to the manufacturer's recommendations.[35]

Dual-Luciferase Reporter Assay

We used the miRcode algorithm (release 6.2, http://www.mircode.org/) to search for miR-RNA target of RELA. The wild or mutated RELA was developed by PCR from human genomic DNA. For the luciferase reporter assay, the pmirGLO dual-luciferase miRNA target expression vector (psiCHECK2-RELA-3′ UTR, psiCHECK2-RELA-3′ UTR-Mut) was used. The oligonucleotide sequences (WT) used are shown in Table S4. The luciferase reporter assay was performed using the Dual-Luciferase reporter assay system (Promega). The luciferase activity was measured 48 h after transfection.[36,37]

ChIP-PCR assay

The ChIP-PCR assay was performed in MDA-MB-231 cells with SimpleChIP assay kits (Beyotime Institute of Biotechnology, Hangzhou,

China; Cell Signaling Technology) as described previously.[33,34] The primers used in the ChIP assay are listed in Table S5.

Histopathology

Thirty-one days after mice were challenged by Lentivector-LD-BCSCs, Lenti-miR-7- LD-BCSCs, or Lentivector-LD-BCSCs, mice were sacrificed and the lung tissues were fixed in 10% formalin and then embedded in paraffin. Serial thin tissue sections (5 μm) were cut and mounted on SuperFrost Plus glass slides, fixed in methanol, and stained in H&E. The slides were viewed under a Zeiss Axioplan light microscope at a magnification of ×100, ×200, or ×400.[35,38]

Immunohistochemical Staining

Briefly, 5-μm-thick formalin-fixed and paraffin-embedded slides were incubated with a rabbit anti-mouse/human E-cadherin (20874-1-AP) (Proteintech, USA) and anti-mouse/human vimentin (5741s) (Cell Signaling Technology, USA) overnight at 4°C. The samples were then labeled with horseradish peroxidase-conjugated streptavidin (Invitrogen), and the chromogenic reaction was developed using a liquid diaminobenzidine (DAB) substrate pack according to the manufacturer's instructions. The stained cells from random and non-overlapping fields were counted under a magnification of ×200.[39,40]

Assays of Cell Proliferation, Colony, and Migration

2×10^3 siESAM-1-, siESAM-2-, and siESAM-3-transfected MDA-MB-231 cells or MDA-MB-231 cell suspensions seeded into 96-well plates were assayed for proliferative activity in triple wells and colony formation. A colony with a diameter larger than 75 μm or having more than 50 cells was counted for one positive colony according to our previous report.[23] In migration assay, the same above-mentioned cells were plated in six-well plates (5×10^5 cells per well) to form a monolayer 1 day before the assay. The subsequent steps were performed as previously described.[30]

Statistical Analysis

Statistical analyses were performed using the Student's t test or single factor analysis of variance to test for the difference between the experimental and the control groups. The mean and standard deviations of the results between the two groups were used and p values <0.05 were taken as statistically significant.

SUPPLEMENTAL INFORMATION

Supplemental Information can be found online at https://doi.org/10.1016/j.omto.2020.06.002.

AUTHOR CONTRIBUTIONS

M.L, M.P., J.W., and J.D. designed and carried out the experiments, data analysis, and manuscript writing; J.W. and C.Y. collected clinical samples; F.Z. and D.Z. performed real-time PCR and western blotting assays; M.G., H.X., D.W., and L.W. performed animal models and flow cytometry; J.D. provided overall supervision; and all authors read and approved the final manuscript.

CONFLICTS OF INTEREST

The authors declare no competing interests.

ACKNOWLEDGMENTS

The study has been supported by the National Natural Science Foundation of China (no. 81572887); the Scientific Research Foundation of the Graduate School of Southeast University (YBJJ1746); the Foundation of Nanjing Science and Technology Development Plan (2016sc512020); the Scientific Research Foundation of Southeast University (2242019k40258); and partly supported by the National Key Research and Development Program of China (2017YFA0205502).

REFERENCES

1. de Boniface, J., Schmidt, M., Engel, J., Smidt, M.L., Offersen, B.V., and Reimer, T. (2018). What is the best management of cN0pN1(sn) breast cancer patients? Breast Care (Basel) *13*, 331–336.

2. Choi, H.S., Kim, S.L., Kim, J.H., Deng, H.Y., Yun, B.S., and Lee, D.S. (2018). Triterpene acid (*3-O-p*-coumaroyltormentic acid) isolated from aronia extracts inhibits breast cancer stem cell formation through downregulation of c-Myc protein. Int. J. Mol. Sci. *19*, 2528.

3. Gkountela, S., Castro-Giner, F., Szczerba, B.M., Vetter, M., Landin, J., Scherrer, R., Krol, I., Scheidmann, M.C., Beisel, C., Stirnimann, C.U., et al. (2019). Circulating tumor cell clustering shapes DNA methylation to enable metastasis seeding. Cell *176*, 98–112.e14.

4. Zhou, H., Yu, C., Kong, L., Xu, X., Yan, J., Li, Y., An, T., Gong, L., Gong, Y., Zhu, H., et al. (2019). B591, a novel specific pan-PI3K inhibitor, preferentially targets cancer stem cells. Oncogene *38*, 3371–3386.

5. Zhou, J., Zhang, H., Gu, P., Margolick, J.B., Yin, D., and Zhang, Y. (2009). Cancer stem/progenitor cell active compound 8-quinolinol in combination with paclitaxel achieves an improved cure of breast cancer in the mouse model. Breast Cancer Res. Treat. *115*, 269–277.

6. Dou, J. (2017). Cancer stem cells are the origins of tumor growth and recurrences. Chin. Sci. Bull. *62*, 1806–1814.

7. Ishida, T., Kundu, R.K., Yang, E., Hirata, K., Ho, Y.D., and Quertermous, T. (2003). Targeted disruption of endothelial cell-selective adhesion molecule inhibits angiogenic processes in vitro and in vivo. J. Biol. Chem. *278*, 34598–34604.

8. Cangara, H.M., Ishida, T., Hara, T., Sun, L., Toh, R., Rikitake, Y., Kundu, R.K., Quertermous, T., Hirata, K., and Hayashi, Y. (2010). Role of endothelial cell-selective adhesion molecule in hematogeneous metastasis. Microvasc. Res. *80*, 133–141.

9. Kacso, T., Bondor, C.I., Rusu, C.C., Moldovan, D., Trinescu, D., Coman, L.A., Ticala, M., Gavrilas, A.M., and Potra, A.R. (2018). Adiponectin is related to markers of endothelial dysfunction and neoangiogenesis in diabetic patients. Int. Urol. Nephrol. *50*, 1661–1666.

10. Okuda, H., Xing, F., Pandey, P.R., Sharma, S., Watabe, M., Pai, S.K., Mo, Y.Y., Iiizumi-Gairani, M., Hirota, S., Liu, Y., et al. (2013). miR-7 suppresses brain metastasis of breast cancer stem-like cells by modulating KLF4. Cancer Res. *73*, 1434–1444.

11. Zhang, H., Cai, K., Wang, J., Wang, X., Cheng, K., Shi, F., Jiang, L., Zhang, Y., and Dou, J. (2014). miR-7, inhibited indirectly by lincRNA HOTAIR, directly inhibits SETDB1 and reverses the EMT of breast cancer stem cells by downregulating the STAT3 pathway. Stem Cells *32*, 2858–2868.

12. Ozawa, T., Arora, S., Szulzewsky, F., Juric-Sekhar, G., Miyajima, Y., Bolouri, H., Yasui, Y., Barber, J., Kupp, R., Dalton, J., et al. (2018). A de novo mouse model of C11orf95-RELA fusion-driven ependymoma identifies driver functions in addition to NF-κB. Cell Rep. *23*, 3787–3797.

13. Mu, C., Wu, X., Zhou, X., Wolfram, J., Shen, J., Zhang, D., Mai, J., Xia, X., Holder, A.M., Ferrari, M., et al. (2018). Chemotherapy sensitizes therapy-resistant cells to mild hyperthermia by suppressing heat shock protein 27 expression in triple-negative breast cancer. Clin. Cancer Res. *24*, 4900–4912.

14. Wang, J., Chen, D., Shi, F., Chen, J., Zhang, Y., Shi, F., Wu, D., Li, M., Pan, M., and Dou, J. (2016). Mir-200c inhibits HOTAIR expression resulting in the decrease of chemoresistance in ovarian cancer stem cells. Int. J. Clin. Exp. Med. *9*, 13783–13792.

15. Zhou, L., Sheng, D., Wang, D., Ma, W., Deng, Q., Deng, L., and Liu, S. (2019). Identification of cancer-type specific expression patterns for active aldehyde dehydrogenase (ALDH) isoforms in ALDEFLUOR assay. Cell Biol. Toxicol. *35*, 161–177.

16. Kao, J., Salari, K., Bocanegra, M., Choi, Y.L., Girard, L., Gandhi, J., Kwei, K.A., Hernandez-Boussard, T., Wang, P., Gazdar, A.F., et al. (2009). Molecular profiling of breast cancer cell lines defines relevant tumor models and provides a resource for cancer gene discovery. PLoS ONE *4*, e6146.

17. Yang, J., Xu, J., e, Y., and Sun, T. (2019). Predictive and prognostic value of circulating blood lymphocyte subsets in metastatic breast cancer. Cancer Med. *8*, 492–500.

18. Ghader, A., Ardakani, A.A., Ghaznavi, H., Shakeri-Zadeh, A., Minaei, S.E., Mohajer, S., and Ara, M.H.M. (2018). Evaluation of nonlinear optical differences between breast cancer cell lines SK-BR-3 and MCF-7; an in vitro study. Photodiagn. Photodyn. Ther. *23*, 171–175.

19. Ejlertsen, B., Tuxen, M.K., Jakobsen, E.H., Jensen, M.B., Knoop, A.S., Højris, I., Ewertz, M., Balslev, E., Danø, H., Vestlev, P.M., et al. (2017). Adjuvant cyclophosphamide and docetaxel with or without epirubicin for early TOP2A-normal breast cancer: DBCG 07-READ, an open-label, phase III, randomized trial. J. Clin. Oncol. *35*, 2639–2646.

20. Ishibashi, T., Yokota, T., Tanaka, H., Ichii, M., Sudo, T., Satoh, Y., Doi, Y., Ueda, T., Tanimura, A., Hamanaka, Y., et al. (2016). ESAM is a novel human hematopoietic stem cell marker associated with a subset of human leukemias. Exp. Hematol *44*, 269–281.e1.

21. Chen, J., Wang, J., Chen, D., Yang, J., Yang, C., Zhang, Y., Zhang, H., and Dou, J. (2013). Evaluation of characteristics of $CD44^{+}CD117^{+}$ ovarian cancer stem cells in three dimensional basement membrane extract scaffold versus two dimensional monocultures. BMC Cell Biol. *14*, 7.

22. Al-Hajj, M., Wicha, M.S., Benito-Hernandez, A., Morrison, S.J., and Clarke, M.F. (2003). Prospective identification of tumorigenic breast cancer cells. Proc. Natl. Acad. Sci. USA *100*, 3983–3988.

23. Dou, J., Pan, M., Wen, P., Li, Y., Tang, Q., Chu, L., Zhao, F., Jiang, C., Hu, W., Hu, K., and Gu, N. (2007). IsoClation and identification of cancer stem-like cells from murine melanoma cell lines. Cell. Mol. Immunol. *4*, 467–472.

24. Wang, J., Cao, M.G., You, C.Z., Wang, C.L., Liu, S.L., Kai, C., and Dou, J. (2012). A preliminary investigation of the relationship between circulating tumor cells and cancer stem cells in patients with breast cancer. Cell. Mol. Biol. (Noisy-le-grand) *58* (*Suppl*), 1641–1645.

25. Li, C.L., Leng, Y., Zhao, B., Gao, C., Du, F.F., Jin, N., Lian, Q.Z., Xu, S.Y., Yan, G.L., Xia, J.J., et al. (2017). Human iPSC-MSC-derived xenografts modulate immune responses by inhibiting the cleavage of caspases. Stem Cells *35*, 1719–1732.

26. Tong, Q., Wang, X.L., Li, S.B., Yang, G.L., Jin, S., Gao, Z.Y., and Liu, X.B. (2018). Combined detection of IL-6 and IL-8 is beneficial to the diagnosis of early stage esophageal squamous cell cancer: a preliminary study based on the screening of serum markers using protein chips. OncoTargets Ther. *11*, 5777–5787.

27. Yin, J.Y., Huo, J.S., Ma, X.X., Sun, J., and Huang, J. (2017). Study on the simultaneously quantitative detection for β-lactoglobulin and lactoferrin of cow milk by using protein chip technique. Biomed. Environ. Sci. *30*, 875–886.

28. Hu, W., Wang, J., Dou, J., He, X., Zhao, F., Jiang, C., Yu, F., Hu, K., Chu, L., Li, X., and Gu, N. (2011). Augmenting therapy of ovarian cancer efficacy by secreting IL-21 human umbilical cord blood stem cells in nude mice. Cell Transplant. *20*, 669–680.

29. Wu, D., Yu, X., Wang, J., Hui, X., Zhang, Y., Cai, Y., Ren, M., Guo, M., Zhao, F., and Dou, J. (2019). Ovarian cancer stem cells with high ROR1 expression serve as a new prophylactic vaccine for ovarian cancer. J. Immunol. Res. *2019*, 9394615.

30. Chen, D., Zhang, Y., Wang, J., Chen, J., Yang, C., Cai, K., Wang, X., Shi, F., and Dou, J. (2013). MicroRNA-200c overexpression inhibits tumorigenicity and metastasis of $CD117^{+}CD44^{+}$ ovarian cancer stem cells by regulating epithelial-mesenchymal transition. J. Ovarian Res. *6*, 50.

31. Dou, J., Wang, Y., Yu, F., Yang, H., Wang, J., He, X., Xu, W., Chen, J., and Hu, K. (2012). Protection against *Mycobacterium tuberculosis* challenge in mice by DNA vaccine Ag85A-ESAT-6-IL-21 priming and BCG boosting. Int. J. Immunogenet. *39*, 183–190.

32. Wang, X., Zhao, F., He, X., Wang, J., Zhang, Y., Zhang, H., Ni, Y., Sun, J., Wang, X., and Dou, J. (2015). Combining TGF-β1 knockdown and miR200c administration to optimize antitumor efficacy of B16F10/GPI-IL-21 vaccine. Oncotarget *6*, 12493–12504.

33. Ceol, C.J., Houvras, Y., Jane-Valbuena, J., Bilodeau, S., Orlando, D.A., Battisti, V., Fritsch, L., Lin, W.M., Hollmann, T.J., Ferré, F., et al. (2011). The histone methyltransferase SETDB1 is recurrently amplified in melanoma and accelerates its onset. Nature *471*, 513–517.

34. Zhang, H.F., Chen, Y., Wu, C., Wu, Z.Y., Tweardy, D.J., Alshareef, A., Liao, L.D., Xue, Y.J., Wu, J.Y., Chen, B., et al. (2016). The opposing function of STAT3 as an oncoprotein and tumor suppressor is dictated by the expression status of STAT3β in esophageal squamous cell carcinoma. Clin. Cancer Res. *22*, 691–703.

35. Rosenberg, S.A., Sherry, R.M., Morton, K.E., Scharfman, W.J., Yang, J.C., Topalian, S.L., Royal, R.E., Kammula, U., Restifo, N.P., Hughes, M.S., et al. (2005). Tumor progression can occur despite the induction of very high levels of self/tumor antigen-specific $CD8^{+}$ T cells in patients with melanoma. J. Immunol. *175*, 6169–6176.

36. Harrow, J., Frankish, A., Gonzalez, J.M., Tapanari, E., Diekhans, M., Kokocinski, F., Aken, B.L., Barrell, D., Zadissa, A., Searle, S., et al. (2012). GENCODE: the reference human genome annotation for The ENCODE Project. Genome Res. *22*, 1760–1774.

37. Chiyomaru, T., Yamamura, S., Fukuhara, S., Yoshino, H., Kinoshita, T., Majid, S., Saini, S., Chang, I., Tanaka, Y., Enokida, H., et al. (2013). Genistein inhibits prostate cancer cell growth by targeting miR-34a and oncogenic HOTAIR. PLoS ONE *8*, e70372.

38. Hu, K., Dou, J., Yu, F., He, X., Yuan, X., Wang, Y., Liu, C., and Gu, N. (2011). An ocular mucosal administration of nanoparticles containing DNA vaccine pRSC-gD-IL-21 confers protection against mucosal challenge with herpes simplex virus type 1 in mice. Vaccine *29*, 1455–1462.

39. Wang, X., He, X., Zhao, F., Wang, J., Zhang, H., Shi, F., Zhang, Y., Cai, K., and Dou, J. (2014). Regulation gene expression of miR200c and ZEB1 positively enhances effect of tumor vaccine B16F10/GPI-IL-21 on inhibition of melanoma growth and metastasis. J. Transl. Med. *12*, 68.

40. Yang, C., Xiong, F., Wang, J., Dou, J., Chen, J., Chen, D., Zhang, Y., Luo, S., and Gu, N. (2014). Anti-ABCG2 monoclonal antibody in combination with paclitaxel nanoparticles against cancer stem-like cell activity in multiple myeloma. Nanomedicine (Lond.) *9*, 45–60.